Volume 1 | Number 1 | Jan 2013 | Pages 1–100

ChemComm

Chemical Communications
www.rsc.org/chemcomm

ROYAL SOCIETY OF CHEMISTRY

This is an *Accepted Manuscript*, which has been through the Royal Society of Chemistry peer review process and has been accepted for publication.

Accepted Manuscripts are published online shortly after acceptance, before technical editing, formatting and proof reading. Using this free service, authors can make their results available to the community, in citable form, before we publish the edited article. We will replace this *Accepted Manuscript* with the edited and formatted *Advance Article* as soon as it is available.

You can find more information about *Accepted Manuscripts* in the **Information for Authors**.

Please note that technical editing may introduce minor changes to the text and/or graphics, which may alter content. The journal's standard **Terms & Conditions** and the **Ethical guidelines** still apply. In no event shall the Royal Society of Chemistry be held responsible for any errors or omissions in this *Accepted Manuscript* or any consequences arising from the use of any information it contains.

www.rsc.org/chemcomm

Chemical Communications

COMMUNICATION

A New Lithium-Rich Anti-Spinel in Li-O-Br System

J. Zhang,[a] J. Zhu[b], L. Wang[b] and Y. Zhao[b]

Abstract: In spinel-type materials currently known, the divalent anions are arranged in a closed-pack lattice and cations of various valences occupy some or all of the tetrahedral and octahedral sites. We report here the first discovery of an "electronically inverted" anti-spinel. The new material, crystallized in a defect spinel structure, was obtained from the dehydration of $Li_5Br(OH)_4$ under moderate pressure and temperature conditions.

The spinel structure is a common structure in a wide variety of crystalline materials. The general composition for the spinel structure is AB_2X_4, derived from mineral spinel $MgAl_2O_4$, which crystallizes in the space group of *Fd-3m* (227). In a normal AB_2X_4 spinel, the A ions are in the tetrahedral $8(a)$ sites and the B ions are in the octahedral $16(d)$ sites. The spinel structure is flexible with regard to the distribution of A and B ions at tetrahedral and octahedral sites. When A ions occupy one half of the octahedral sites and B ions occupy the other half of the octahedral and all tetrahedral sites, the structure is called inverse spinel, generally expressed as $B[AB]X_4$ (*e.g.*, $Fe^{3+}[Fe^{2+}Fe^{3+}]O_4$ magnetite). There are yet a third family of materials crystallized in the defect spinel structure, best known in γ–Fe_2O_3 [ref 1] and γ–Al_2O_3 [ref 2]. In γ–Fe_2O_3, for example, one sixth of Fe^{3+} at the $16(d)$ sites are vacant to compensate charge, resulting in a defect spinel $[Fe^{3+}]_{IV}[\square_{1/3}Fe^{3+}_{5/3}]_{VI}O_4$, indicating that the spinel structure can accommodate a substantially large amount of vacancies in the crystal lattice (denoted by $\square$ in the chemical formula). In all known materials that exhibit the spinel structure, both A and B ions are cations and X is an electronegative divalent anion such as O^{2-} and S^{2-}. However, despite its flexibility to a wide range of compositions and vacancies, the spinel structure with inverted cation and anion positions, the so-called anti-spinel, has yet been reported in any material system.

The new anti-spinel was synthesized in the system Li-O-Br under pressures (*P*) less than 2 GPa and temperatures (*T*) below 330 ºC. The starting material has a 2:1 molar ratio of Li_2O:LiBr. The synthesis processes were monitored by *in-situ* and *real-time* synchrotron x-ray diffraction. In spite of all cautions in isolating the starting reagents from room air, they can readily react with air moisture to form $Li_5Br(OH)_4$ via the reaction $2Li_2O + LiBr + H_2O = Li_5Br(OH)_4$, when the pressure cell was transported from glove box to the hydraulic press. As a result, the high *P-T* synchrotron experiment was performed on monoclinic $Li_5Br(OH)_4$ rather than a mixture of Li_2O and LiBr. More related experimental detail and discussion can be found in ref. [3].
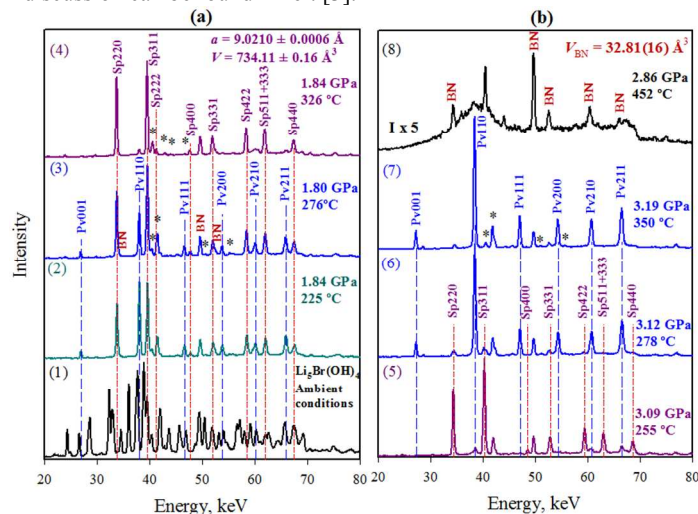

Figure 1 Selected x-ray diffraction patterns obtained during the initial heating cycle around 1.8 GPa (*left panel*) and 4th and last heating cycle around 3 GPa that led to the melting of anti-perovskite Li_3OBr (*right panel*). Between the two cycles, similar patterns were observed for the *Sp* → *Pv* conversion at 3.6 GPa/250 ºC during

second heating and for the *Pv → Sp* conversion at 2.3 GPa/325 °C during third heating. A subset of impurity diffraction lines, denoted as BN, are from hexagonal boron nitride, which was used as the sample container and also for separating the sample from NaCl pressure standard. The remaining impurity reflections, denoted by asterisks, are from high-pressure phase of LiOH (see Figure 2 and footnotes for more detail). Diffraction intensities in patterns #2-7 are normalized with respect to the data counting time, and they are multiplied by five in pattern #8.

Figure 1a shows selected diffraction data collected during the initial heating cycle. At 1.84 GPa/225 °C, the obtained diffraction pattern (pattern #2) is drastically different from that of the starting $Li_5Br(OH)_4$ (pattern #1). A subset of reflections can be indexed by space group *Pm-3m* (221) for anti-perovskite Li_3OBr[3, 4], thereafter denoted as *Pv*. Several weaker reflections (denoted by asterisks), notably near photon energies of 40-42 keV or *d*-spacing of 2.56 – 2.68 Å, can be best matched by $I4_1/acd$ Li(OH) (see footnotes for more detail). The remaining diffraction lines, however, do not match any other known phases in the system Li-Br-O-H. Upon further heating, the new phase continued to form at the expense of anti-perovskite Li_3OBr (pattern #3) and became dominant at 1.84 GPa/326 °C (pattern #4). At those conditions, as summarized in the Table 1 of footnotes, all strong reflections can be well indexed by space group *Fd-3m* (227), indicating that the new phase is isostructured with the common $MgAl_2O_4$ spinel, which is thereafter denoted as *Sp*. These observations also indicate that anti-perovskite is an intermediate and metastable phase. However, the simultaneous appearance of the anti-perovskite and new spinel phases at the early stage of heating (pattern #2) suggests that the two phases may be separated by rather small energies.

The spinel phase formed at 1.84 GPa/326 °C (i.e., pattern #4 of Figure 1a) can be recovered under pressure during fast cooling to room temperature. In Figure 1b, we show diffraction patterns obtained in the subsequent experimental steps when spinel phase was further compressed and then re-heated at higher pressures around 3 GPa (fourth and last heating cycle of the experiment). With increasing temperature from 255 °C (pattern #5) to 278 °C (pattern #6), the spinel phase was almost entirely transformed to anti-perovskite, which is structurally stable until it melts at 2.86 GPa and 452 °C (patterns #7 and #8). Between the first (Fig 1a) and last (Fig 1b) heating cycles, the transitions between anti-perovskite and spinel phases were also observed upon heating under different pressure conditions, 3.61 GPa/250 °C for *Sp → Pv* during second heating cycle and 2.32 GPa/325 °C for *Pv → Sp* during third heating cycle. Based on these observations, *Pm-3m* anti-perovskite is energetically more stable than *Fd-3m* spinel at pressures approximately above 2.5 GPa. Our finding supports previous first-principles calculations in that the anti-perovskite Li_3OBr is a metastable phase at ambient pressure[5, 6].

Figure 2 shows the Le Bail fit of the diffraction pattern collected at 2.32 GPa and 325 °C. The observed data from the sample material can be nicely fit by *Fd-3m* spinel, anti-perovskite Li_3OBr and $I4_1/acd$ Li(OH). Based on the starting compositions and in-situ x-ray

observations described in the preceding paragraphs, the new spinel phase, in the form of Li_3OBr, was initially formed via the following dehydration reaction

$$Li_5Br(OH)_4 = Li_3OBr \ (sp) + 2LiOH + H_2O \qquad (1)$$

In the subsequent experimental steps, the reversibility of phase transition between spinel and perovskite of the known composition (Li_3OBr) and the lack of evidence for disproportional reaction during transition further suggest that the two phases are isochemical.
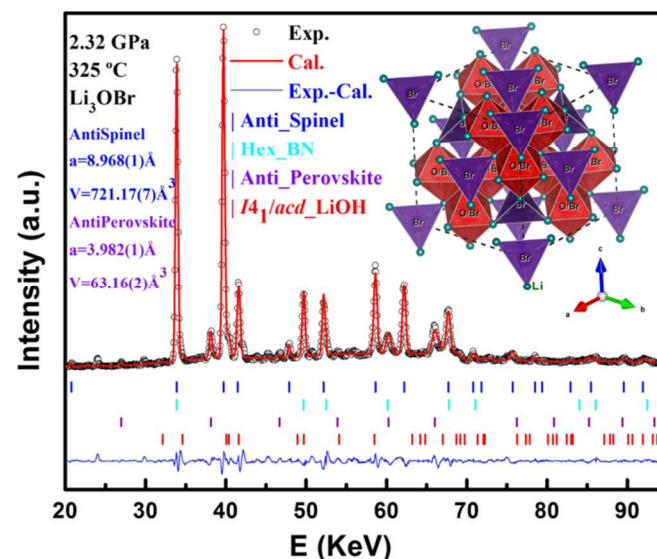

Figure 2 Le Bail fit of the observed pattern at 2.32 GPa and 325 °C. The inset shows the crystal structure of anti-spinel with space group *Fd-3m*.

It is unusual in several aspects for Li_3OBr to crystallize in the spinel structure. Firstly, it is a defect spinel per a general AB_2X_4 formula. Although uncommon, defect spinels in the form of ABX_3 have been reported previously in several material systems. In addition to the aforementioned γ–Fe_2O_3 [ref 1] and γ–Al_2O_3 [ref 2], several ABO_3 oxides also crystallize in the defect spinel structure, including $ATiO_3$ oxides with A = Zn and Co[7] and $AMoO_3$ oxides with A = Mn, Co and Zn[8]. For an ABX_3 composition to crystallize in a conventional spinel structure, the compound must have 1/3 cation vacancies at either the tetrahedral or octahedral sites per AB_2X_4 formula. Materials with a defect spinel structure can be obtained by a variety of chemical routes, such as dehydration of FeOOH for γ–Fe_2O_3 [ref 9] and hydrogen-reduction of $AMoO_4$ for $AMoO_3$ oxides[10]. They are often metastable at ambient conditions and transform to thermodynamically stable phases under thermal (*e.g.*, γ–Fe_2O_3 → α–Fe_2O_3, ref. 10) or mechanical treatment (*e.g.*, γ–Al_2O_3 → α–Al_2O_3, ref. 11). Secondly, it is an "electronically inverted" anti-spinel, which, to the best of our knowledge, has yet been reported in literature. In the Li_3OBr anti-spinel, as shown in the inset of Figure 2, the anion X in the conventional AB_2X_4 system is replaced by the electropositive lithium ion, located at the tetrahedral vertices. To continue electronic inversion, both A and B cations are replaced by electronegative ions, namely Br^{-1} and O^{-2}, which, based on our simulations discussed below, are distributed in the tetrahedral and

octahedral sites corresponding to an inverse spinel. In literature, the inverse spinel is sometimes referred to as anti-spinel [*e.g.*, ref 12]. This terminology, however, is inappropriate in the context of the present findings. As a result of the anti-spinel nature, the new spinel phase is presumably most enriched in lithium among the known oxide spinels on the basis of one oxygen atom in a chemical formula, and it is thereafter denoted as LiRAS, standing for Li-Rich Anti-Spinel. In addition, the measured lattice constant of LiRAS, $a = 9.021$ Å (see Table 1 of the footnotes), is 7-12% larger than those of lithium-based transition-metal oxides, commonly in the range of 8.0 – 8.4 Å when crystallized in the spinel structure[13]. The expanded lattice space would in principle facilitate ionic transport in the crystal for interstitial ions[5].
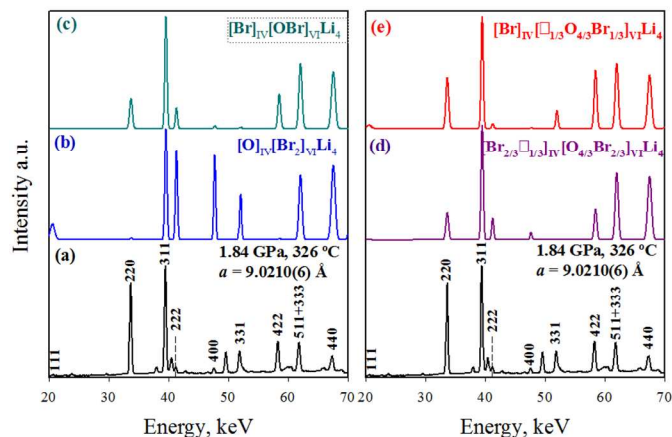

Figure 3 Observed (*a*) and simulated x-ray patterns (*b* − *e*) for anti-spinel structure of various anion and vacancy distributions. All simulated patterns were generated by using a GSAS+ExpGUI software package with space group *Fd-3m* and a lattice parameter of 9.02 Å. The fractional coordinates of Li, O and Br atoms are (0.3692, 0.3692, 0.3692), (0.5, 0.5, 0.5) and (0.125, 0.125, 0.125), respectively, for Br ions in the tetrahedral sites and O ions in the octahedral sites. They are (0.7379, 0.7379, 0.7379), (0.5, 0.5, 0.5) and (0.875, 0.875, 0.875), respectively, for O ions in the tetrahedral sites and Br ions in the octahedral sites. An isotropic thermal vibration parameter of 0.025 was used for all atoms.

A number of x-ray patterns were simulated on LiRAS by considering different anion and vacancy distributions for normal, inverse and defect spinel. For the defect Li_3OBr anti-spinel, simulations were performed on $[O]_{IV}[\square_{1/3}O_{1/3}Br_{4/3}]_{VI}Li_4$, $[Br]_{IV}[\square_{1/3}O_{4/3}Br_{1/3}]_{VI}Li_4$, $[Br_{2/3}\square_{1/3}]_{VI}[O_{4/3}Br_{2/3}]Li_4$, and $[O_{2/3}\square_{1/3}]_{VI}[O_{2/3}Br_{4/3}]Li_4$, assuming that the anion vacancies can be in either the tetrahedral or octahedral sites. To compare with defect-free anti-spinel of the conventional AB_2X_4 composition, we also simulated patterns for $[O]_{IV}[Br_2]_{VI}Li_4$ and $[Br]_{IV}[BrO]_{VI}Li_4$. The selected patterns from simulations are shown in Figure 3 and compared with the observed data at 1.84 GPa/326 ºC. Quantitatively speaking, none of the simulated patterns match very well with the observed diffraction intensities in pattern (a). However, for both Li_3OBr and Li_4OBr_2 compositions, simulated patterns for a normal spinel are intolerably mismatched, especially for reflections of (220), (222), (400) and (422), as exemplified in the

pattern (b) for $[O]_{IV}[Br_2]_{VI}Li_4$. Our simulations are thus in favor of an inverse spinel in the system Li-O-Br, indicating that oxygen ions should preferentially occupy the octahedral sites. Among simulated patterns for an inverse anti-spinel (*e.g.*, patterns *d and e*), the one for $[Br]_{IV}[\square_{1/3}O_{4/3}Br_{1/3}]_{VI}Li_4$ (pattern *e*) shows best match with the observed intensities, notably for reflections of (220), (222) and (331), suggesting that in a defect Li_3OBr anti-spinel 1/3 anion vacancies are in the octahedral sites. Further experimental studies, such as neutron diffraction, and computational modelling are warranted for distinction between different structural models.

Conclusions

In this work, we discovered the first anti-spinel structure with inverted cation and anion positions. The new material, crystallized in a defect spinel structure, was obtained through dehydration of $Li_5Br(OH)_4$ under moderate pressure and temperature conditions. In the family of lithium-based oxide spinels, the new anti-spinel has the largest lattice constant for a cubic unit cell. The halogen-based LiRAS may potentially represent a new class of solid electrolytes for lithium-ion battery applications.

Notes and references

[a] Materials Science and Technology Division, Los Alamos National Laboratory, Los Alamos, NM 87545 USA.
[b] High Pressure Science and Engineering Center and Department of Physics and Astronomy, University of Nevada, Las Vegas, NV 89154 USA.

† Footnotes: At ambient conditions LiOH crystallizes in space group *P4/nmm*. With increasing pressure it transforms to a new structure called LiOH-III at 0.7 GPa (or 1.7 GPa in LiOD)[14, 15]. LiOH-III was initially suggested to possess the *Pbcm* symmetry[7] but later reassigned to monoclinic *P21/a* based on room-temperature neutron diffraction data[15]. Most recently, several structure candidates, including *Pbcm*, *P2₁/a*, *I4₁/acd* and *P2₁2₁2₁*, have been proposed for LiOH-III based on first-principles calculations[16]. The *I4₁/acd* structure was singled out to be the most stable ground-state structure between 1 GPa and 16.5 GPa. At higher pressures, the *I4₁/acd* structure was predicted to transform to an additional new phase, LiOH-IV, with the *Pbcm* symmetry. Consistent with first-principles calculations, our Le Bail fits using the *I4₁/acd* structure (see Figure 2 in the main text) show best match with the impurity reflections observed in patterns #2 and #3 in Fig 1a and patterns #5-7 in Fig 1b. For impurity reflections in pattern #4, a better match was

obtained by using the *Pbcm* structure, indicating that there is high-temperature phase transformation in LiOH when temperature was increased at ~1.8 GPa from 276 ºC (pattern #3 in Fig 1a) to 326 ºC (pattern #4 in Fig 1a). Further resolution of the crystal structure or structural controversy for the high-pressure LiOH, however, is beyond the scope of this paper.

Table 1 X-ray diffraction data of the new spinel phase in the system Li-O-H-Br

h k l	d_{obs}, Å	d_{calc}, Å	$d_{obs} - d_{clac}$, Å
2 2 0	3.1899	3.1894	0.0006
3 1 1	2.7207	2.7199	0.0008
2 2 2	2.6045	2.6041	0.0004
4 0 0	2.2560	2.2552	0.0008
3 3 1	2.0696	2.0696	0.0000
4 2 2	1.8414	1.8414	0.0000
5 1 1	1.7359	1.7361	-0.0002
3 3 3	1.7359	1.7361	-0.0002
4 4 0	1.5943	1.5947	-0.0004

Data were obtained at 1.84 GPa and 326 ºC. The lattice constant for a cubic unit cell is $a = 9.0210$ (6) Å or $V = 734.11(16)$ Å^3, which is 37% larger in molar volume than that of the coexisted anti-perovskite [$V = 66.73(8)$ Å^3].

1   V. Petkov, P. D. Cozzoli, R. Buonsanti, R. Cingolani, R. Yang, *J. Am. Chem. Soc*. 2009, **131**, 14264.

2   M. E. Miller and S. T. Misture, *J. Phys. Chem. C* 2010, **114**, 13039.

3   J. Zhang, J. Han, J. Zhu, Z. Lin, M. H. Braga, L. L. Daemen, L. Wang and Y. Zhao, *Inorg. Chem. Comm*. 2014, **48**, 140.

4   Y. Zhao and L. L. Daemen, *J. of Am. Chem. Soc*. 2012, **134**, 15042.

5   Y. Zhang, Y. Zhao and C. Chen, *Phys. Rev. B* **2013**, 87, 134303.

6   A. Emly, E. Kioupakis, and A. Van der Ven, *Chem. Mater*. 2013, **25**, 4663.

7   A. Manthiam and J. Gopalakrishnan, *Mater. Res. Bull*. 1980, **15**, 207.

8   J. C. Joubert, G. Berthet, and E. F. Bertaut, in *Problems of Nonstoichiometry*, ed. Rabenau A. 1970, pp. 179, North-Holland Publ. Co, Amsterdam.

9   U. Schwertmann and R. M. Cornell, *Iron Oxides in the Laboratory: Preparation and Characterization* 1991, pp. 137, VCH.

10   Y. E. Mendili, J. F. Bardeau, N. Randrianantoandro, F. Grasset, J. M. Greneche, *J. Phys. Chem. C* 2012,**116**, 23785.

11   A. Düvel, E. Romanova, M. Sharifi, D. Freude, M. Wark, P. Heitjans, and M. Wilkening, *J. Phys. Cem. C* 2011, **115**, 22770.

12   **R.** Gopalan and V. Ramalingam, *Concise Coordination Chemistry* 2001, pp.422, Sangam Books Ltd.

13   K. Ariyoshi, Y. Makimura, and T. Ohzuku T., in *Lithium Ion Rechargeable Batteries: Materials, Technology, and New Applications*, ed. Kazunori Ozawa 2009, pp.350, Wiley-VCH.

14   D. M. Adams, and J. Haines, *J. Phys. Chem*. 1991, **95**, 7068.

15   D. M. Adams, A. G. Christy, and J. Haines, *J. Phys. Chem*. 1992, **96**, 8173–8176.

16   A. Hermann, N. W. Ashcroft and R. Hoffmann, *J. Chem. Phys*. 2014, **141**, 024505.